JMEPEG (2007) 16:757–765
DOI: 10.1007/s11665-007-9148-6

1059-9495/$19.00

An Investigation of Carbon Content and Consolidation Temperature on Microstructure and Properties of Hafnium Boride Ceramic

T.S. Srivatsan, G. Guruprasad, M. Zelin, R. Radhakrishnan, and T.S. Sudarshan

(Submitted January 26, 2006; in revised form October 31, 2006)

This paper discusses the use of Plasma Pressure Compaction to consolidate hafnium diboride powders. The effect of carbon addition on densification was studied. The influence of consolidation temperature on microstructure, density, and hardness of the bulk sample is presented. The interrelationship between microstructure and properties of the bulk sample are rationalized in light of the intrinsic influence of carbon content and the extrinsic influence of consolidation temperature.

Keywords electron microscopy, metallography, optical microscopy, powder metallurgy

1. Introduction

The desire to keep pace with the rapid advances in technology related to elevated temperatures has provided an impetus to develop materials that can withstand high temperatures while concurrently discharging their functions without an appreciable sacrifice in mechanical properties. The expendable and reusable space vehicles, the next generation of rocket engines, and even the hypersonic spacecraft demand materials and structural components that are capable of withstanding temperatures as high as 1600 °C (Ref 1). This has created a need for the production and availability of materials that can effectively perform, without adequate cooling, at temperatures in excess of 2200 °C. Temperatures above 1600 °C, and gradually approaching and exceeding 2200 °C, are referred to as the ultra high temperature (UHT) regime with the objective of facilitating a differentiation of the unique thermo-mechanical demands put forth by the aerospace applications (Ref 1). The selection of potentially suitable structural materials for use at UHTs must satisfy the fundamental requirements of (a) melting point, (b) structural strength, (c) toughness, (d) oxidation resistance, (e) thermal expansion, and (f) creep (Ref 1). Researchers at the Air Force Wright Aeronautical Laboratories (Ref 2-7) have identified a selection of potentially suitable and appropriate structural materials for use at UHTs in the air breathing engines.

T.S. Srivatsan and **G. Guruprasad,** Division of Materials Science and Engineering, Department of Mechanical Engineering, The University of Akron, Akron, OH 44325-3903; and **M. Zelin**, Goodyear Research Center, Goodyear Tire and Rubber Company, Akron, OH; and **R. Radhakrishnan** and **T.S. Sudarshan**, Materials Modification Inc., 2721-D, Merrilee Dr, Fairfax, VA 22031. Contact e-mail: tsrivatsan@uakron.edu.

The early studies conduced over 30 years ago by researchers at the US Air Force Research laboratories concentrated on a small group of metal borides made from the transition metals of titanium, zirconium, and hafnium (Ref 7-13). The metal diborides (denoted as MB_2), particularly those made from the transition metal hafnium (Hf), are unique materials because they are (i) hard, (ii) have high melting temperatures (~3000 K), (iii) moderate thermal expansion, (iv) good thermal shock resistance, (v) unusually high thermal and electrical conductivities, and (vi) acceptable chemical stability (Ref 14, 15). The linear thermal expansion coefficient of HfB_2 is approximately 8×10^{-6}/°C between 25 °C and 2000 °C while its thermal conductivity is 100 W/mK and electrical conductivity is 300 μΩ cm at room temperature (25 °C) (Ref 14, 16). Selection of this material for use at temperatures in excess of 2000 °C did afford it the privilege of being categorized as an ultra high temperature ceramic (UHTC) (Ref 17). The development of ultra high temperature ceramics (UHTC's) having a combination of high mechanical properties and oxidation resistance at temperatures higher than 1600 °C is of engineering interest and importance. The properties of HfB_2 and its composite counterpart (HfB_2/SiC) were the topic of an investigation for such a purpose (Ref 15). The physical properties of hafnium boride are summarized in Table 1.

The discovery of bulk superconductivity, with a transition temperature of 39 K, for magnesium diboride (Ref 18) provided an impetus for the development of (i) synthesis methods, (ii) microstructural characterization, and (iii) studies of the physical properties of the diboride, more particularly those having a simple AlB_2 type structure. The AlB_2 structure is hexagonal (space group *P6/mmm* with one formula unit per unit cell) and consists of a repeated stacking of a graphite-like boron layer and of a close-packed hafnium (Hf) layer. This results in space filling by trigonal prismatic building blocks whose vertices the hafnium atoms occupy and whose centers are occupied by the boron atoms. As every hafnium atom belongs to 12 trigonal prisms, the composition is simply $Hf_{6/12}B$.

The sintering behavior of HfB_2 has not yet been comprehensively studied and documented in the open literature.

Existing documentation in the open literature is strictly empirical. Compositions of the $MB_{1.9}$ were found to be receptive to sintering and resistant to oxidation (Ref 18). The phase diagram of such a metal boride composition demonstrates a sharp reduction in "incipient melting" when the composition of the metal boride is way off the M:2B ratio (Ref 19). When the atomic ratio of hafnium to boron is 87:13, the melting point of the Hf-B system is minimized at 1880 ± 15 °C. In addition, an unbalanced ratio raises the defect level that is required for obtaining high rate diffusivity in solid-solid reactions and sintering (Ref 19). Since HfB_2 has a wide homogeneity range based on temperature of consolidation and the pressure used, the present investigation examines the influence of carbon as an additive and consolidation temperature on microstructure, density and hardness of bulk samples of hafnium boride (HfB_2) synthesized by the technique of plasma pressure compaction (referred henceforth through this manuscript as P^2C^{TM}).

2. Material Selection

Hafnium boride powders are usually prepared by reduction of HfO_2 and B_2O_3 and a subsequent reaction between hafnium and boron to yield HfB_2. The HfB_2 is then milled to obtain powders below 45 μm in size. However, the powders have an adsorbed oxygen layer, which impedes densification. This barrier must be eliminated to promote and/or enhance diffusion across the particle boundaries. When carbon is added, it tends to react with the oxygen to form carbon dioxide (CO_2). The carbon dioxide is driven off during consolidation due to negative pressure in the chamber. Once the oxygen barrier is eliminated, the occurrence of diffusion is facilitated and the resultant sintering is much faster.

The powders used in the study were purchased commercially and used in the as-received state. The hafnium boride powder (45 μm) was procured from Cerac, Inc. The carbon powder (average size 50-nm) was procured from Alfa Aesar (Ward Hill, MA). The hafnium boride powder was thoroughly blended with varying amounts (in weight percentage) of carbon powder to provide the bulk samples. Four bulk samples were

Table 1 Properties of hafnium boride

Melting point	3250 °C
Density	11.2 g/cm^3
Molecular weight	200.11 g/mol
Crystal structure	Hexagonal

Table 2 Processing conditions and compositions of test samples

Sample ID	Composition	Consolidation temperature, °C	Pressure, MPa	Time, Min
1	HfB2	1850	50	15
2	HfB2 + 0.1% C	1850	50	15
3	HfB2 + 0.5% C	1750	50	15
4	HfB2 + 1.0% C	1850	50	15

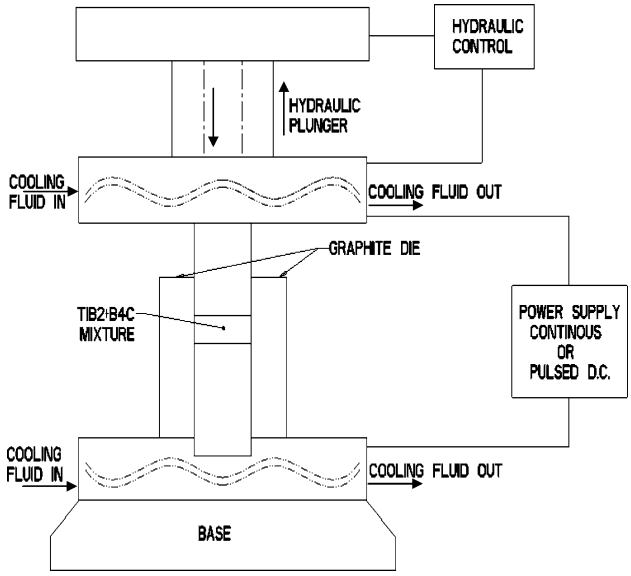

Fig. 1 Schematic showing the plasma pressure compaction (P^2C^{TM}) test set up

Table 3 Density calculation of all samples

Trials	Weight, g	Volume, cm^3	Density, g/cm^3	Average	Relative compaction
Sample 1					
1	18.4504	1.8	10.250	9.594	0.857
2	42.3165	4.3	9.841		
3	37.0391	3.9	9.497		
4	20.2067	2.1	9.622		
5	99.5608	10.9	9.134		
6	118.0112	12.8	9.220		
Sample 2					
1	26.498	2.5	10.599	10.617	0.948
2	39.351	3.7	10.635		
Sample 3					
1	18.388	1.8	10.216	10.245	0.931
2	20.8957	2	10.448		
3	39.2837	3.9	10.073		
Sample 4					
1	26.2617	2.5	10.505	10.599	0.946
2	22.466	2.1	10.698		
3	48.7277	4.6	10.593		

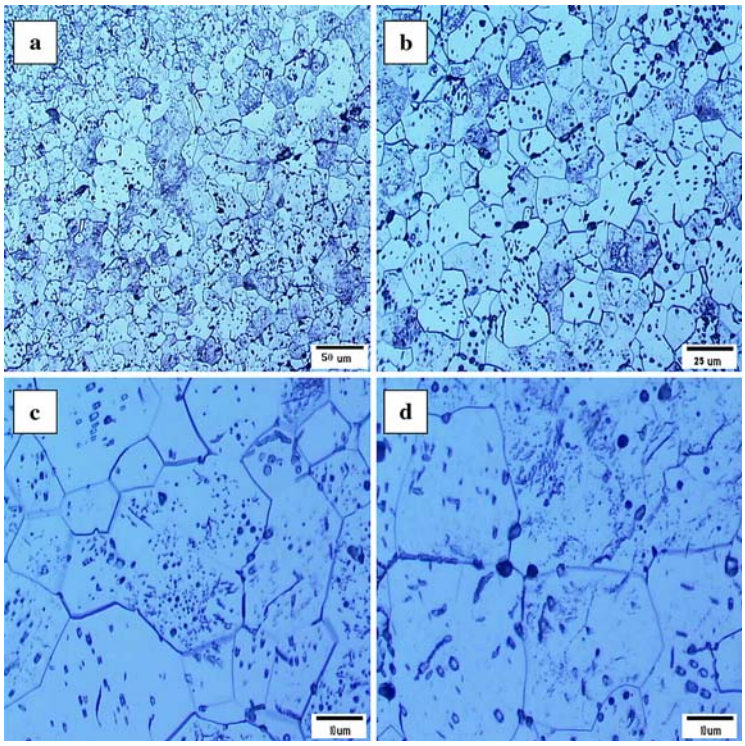

Fig. 2 Optical micrographs of Sample #1 (containing no carbon content) showing: (a) Overall morphology revealing near uniform grain size distribution. (b) High magnification showing the grains to be irregular in shape. (c) Microscopic cracking along the grain boundaries. (d) Random distribution of microscopic voids

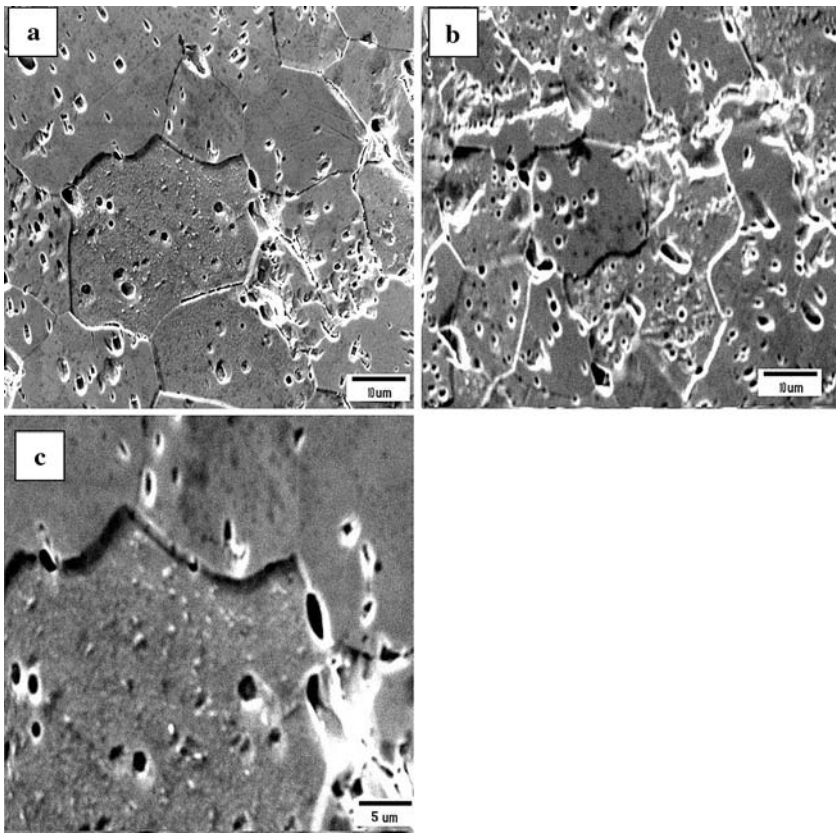

Fig. 3 Scanning electron micrographs of the surface of Sample #1 showing: (a) A population of microscopic voids. (b) Array of fine microscopic cracks distributed through the microstructure. (c) Void coalescence along the grain boundaries

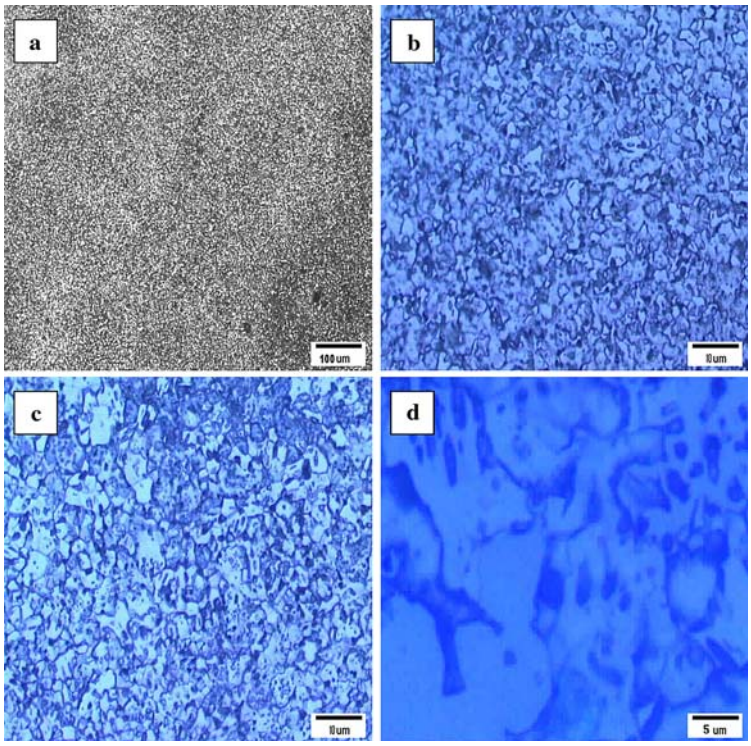

Fig. 4 Optical micrographs of Sample #2 containing 0.1 wt.% carbon, showing: (a) Near uniform grain size distribution at low magnification. (b) High magnification of (a) showing irregular morphology of grains. (c) Microscopic cracks and voids distributed through the microstructure. (d) High magnification of (c) showing numerous voids within an irregular shaped grain

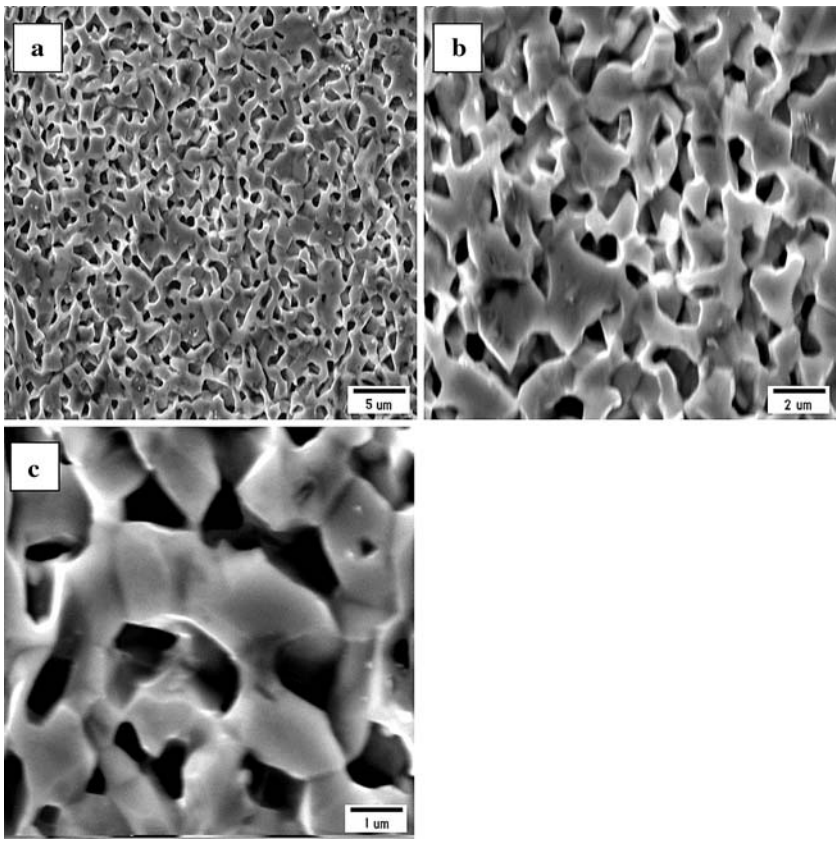

Fig. 5 Scanning electron micrographs of Sample #2 showing the following: (a) Network of microscopic voids. (b) High magnification of (a) revealing a near-fibrous appearance. (c) Microvoid coalescence to form microscopic cracks

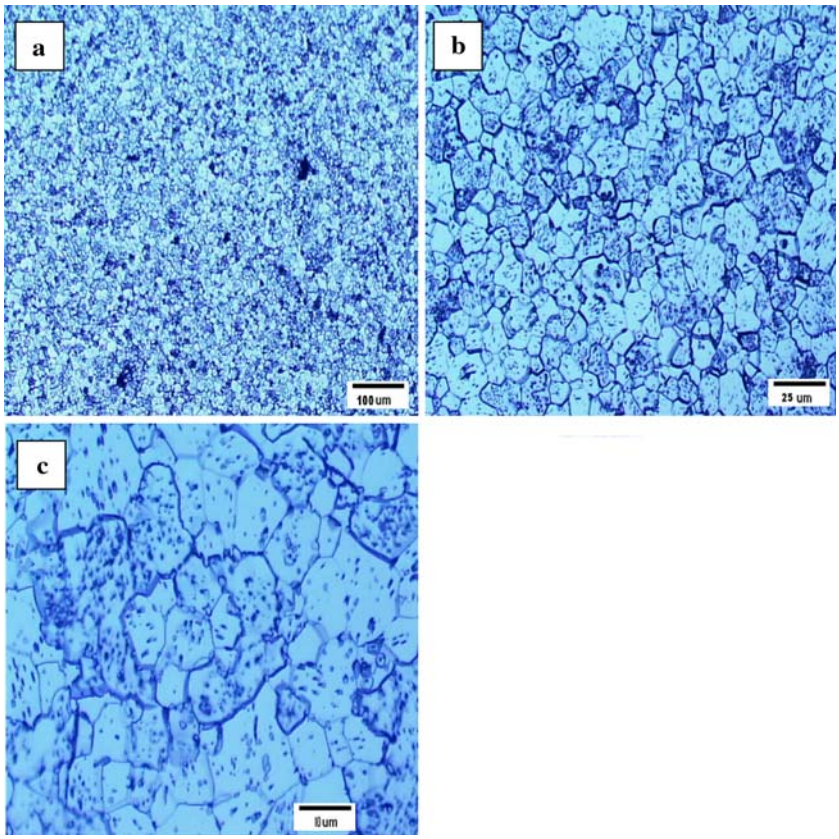

Fig. 6 Bright field optical micrographs of Sample #3 containing 0.5 wt.% carbon, showing (a) A near uniform distribution of grains. (b) High magnification of (a) revealing the grains to be near spherical in shape. (c) Population of voids and random distribution of microscopic cracks

independently prepared by mixing the two powders followed by consolidation:

(A) Sample #1: HfB_2 with no carbon content.
(B) Sample #2: HfB_2 + 0.1 wt.% of carbon.
(C) Sample #3: HfB_2 + 0.5 wt.% of carbon.
(D) Sample #4: HfB_2 + 1.0 wt.% of carbon.

In each case the powder mixture was ball milled for 2 h and subsequently consolidated using the technique of plasma pressure compaction (P^2C^{TM}) (Ref 19-29).

The blended powder mixture was poured into a graphite die. The powder mixture was compressed using graphite plungers. A steady direct current was applied across the powder mixture. The direct current in conjunction with an external pressure of 50 MPa densifies the powder mixture by the mutually interactive influences of resistance heating and the occurrence of localized plastic deformation at the contact surfaces of the powder particles. The resistance heating causes the heat to be concentrated at the interparticle points of contact resulting in an elevation in the local temperature, which is conducive for facilitating diffusion at the microscopic level. The heating rates, reaching as high as 100 °C/min, result in locally high temperatures. For all samples, the consolidation time was 15 min at an externally applied pressure of 50 MPa. The consolidation temperature for three samples (Sample #1, Sample #2, and Sample #4) was chosen to be 1850 °C, and for Sample #3, the consolidation temperature was set at 1750 °C. It was expected that the sintering temperature could be reduced with increasing addition of carbon and that is the reason for consolidating this sample at 1750 °C. The consolidation parameters used for preparing the ceramic samples are summarized in Table 2. A schematic of P^2C^{TM} setup is shown in Fig. 1 (Ref 30).

3. Experimental Procedures

3.1 Initial Characterization of Microstructure

The purpose of characterization of the initial microstructure of the single-phase ceramic samples was to correlate the density and hardness measurements with the intrinsic microstructural features observed in an optical microscope at low magnifications (<1000×), and scanning electron microscope at higher magnifications (>1000×). The as-consolidated samples were mechanically ground and rough polished on progressively finer grades of silicon carbide impregnated emery paper using copious amounts water as coolant and lubricant. The mechanically ground samples were then fine polished to a near mirror-like surface finish using alumina suspended in distilled water as the lubricant. The polished surfaces of the HfB_2 samples were then etched using an etchant (a solution mixture of hydrofluoric acid (10 mL) + nitric acid (30 mL) + hydrogen peroxide (30 mL) + distilled water (50 mL)) for 20 s. The polished and etched surfaces of the samples were observed in an optical microscope and photographed using bright field illumination to determine the following:

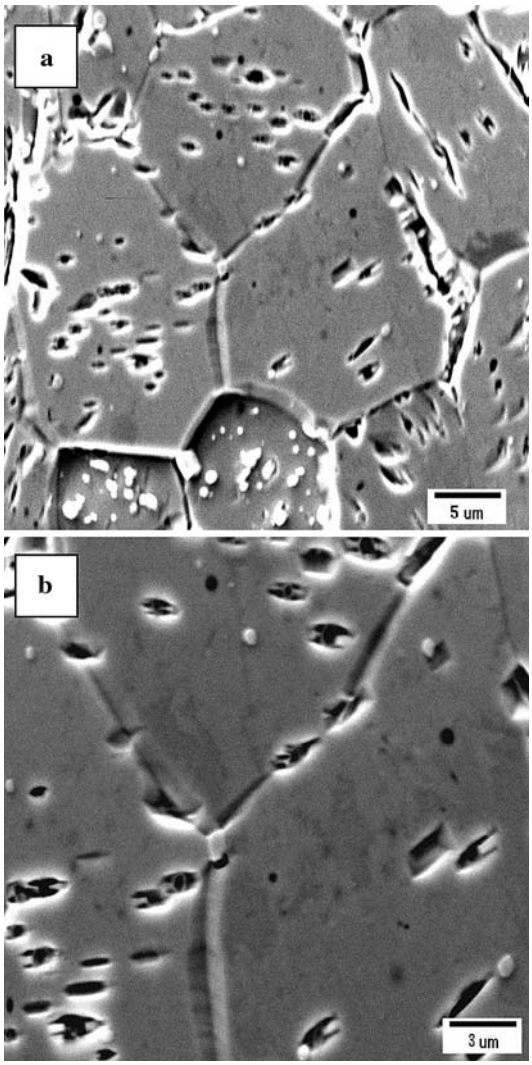

Fig. 7 Scanning electron micrographs of the surface of Sample #3 showing: (a) Cracking along the grain boundaries and a population of voids. (b) Microvoid coalescence at grain boundary regions to form microscopic cracks

1. Size, shape, and orientation of grains
2. The presence, morphology, and distribution of fine microscopic cracks, if any, on the sample surface.
3. Size, morphology, and distribution of the phases, i.e., HfB_2 and carbon.
4. Presence, shape, and location of other processing-related artifacts in the microstructure.

3.2 Indentation Hardness

Hardness is a quantifiable mechanical property of a material. It is a measure of resistance of the chosen ceramic material to indentation, densification, and cracking (Ref 31). Microhardness testing is capable of providing useful information on hardness characteristics of brittle solids that cannot be easily determined using a macroscopic hardness test, such as: Brinell and Rockwell. In this experiment, the Knoop microhardness of the samples was measured. The Knoop hardness value was determined by measuring the size of the indent using a low magnification microscope attached to the indenter. A diamond pyramid indenter was used and length of the indent, i.e., diagonal, on the sample surface was measured. The indentation load used was 500 g for a dwell time of 10 s. Five indents were made on the polished surface of each sample and the result reported is the average value.

3.3 Density Measurements

Measurement of density of each of the four samples was made using the Archimedes's Principle. The weight of each sample specimen was measured to an accuracy of micrograms. The sample was subsequently immersed in distilled water and the volume of water displaced recorded. The ratio of mass of sample to the volume of fluid (water) displaced gives the density.

4. Results and Discussion

4.1 Density

The density was calculated using Archimedes's principle. The initial weight of each sample was measured and the volume of fluid displaced by the corresponding sample was determined by immersion in a beaker containing distilled water. The ratio of weight to volume gives the density of the sample. Several trials were conducted for each sample and the final reported density is the average of three trials. All of the measurements are tabulated in Table 3. Sample# 1 containing no carbon had a density of 9.6 g/cm^3 when compared to the theoretical density of 11.2 g/cm^3. This reveals the relative compaction of this sample to be only 86%. Sample #2 had an average density of 10.6 g/cm^3 when compared to the theoretical density of 11.2 revealing a relative compaction of 95%. The presence of 0.1% carbon has certainly increased the compaction effectiveness and response of the powder mixture (HfB_2 and C). Sample #3 containing 0.5% C had an average density of 10.6 g/cm^3 with a relative compaction of 93%. Sample #4 had an average density of 10.25 g/cm^3 and relative compaction of 95%. It is to be noted that Sample #3 consolidated at the lower temperature (1750 °C) shows good microhardness as well as having achieved good compaction even though it has less carbon content.

4.2 Microstructure

The etched surfaces of the hafnium boride samples were examined in an optical microscope at low magnifications, and a scanning electron microscope at higher magnifications. Overall morphology of the microstructure of this single-phase ceramic revealed the following: (a) the morphology and size of grains, (b) the size, morphology and distribution of phases present in the microstructure, and (c) the presence of processing-related defects such as pores, voids, and microscopic cracks.

4.2.1 Sample #1 (HfB_2, 0% Carbon). At low magnification (<200×), the matrix of this ceramic sample revealed a near uniform grain size distribution (Fig. 2a). At higher magnifications of the optical microscope the grain morphology was observed to be irregular **(**Fig. 2b). High magnification observations also revealed (i) fine microscopic cracking along the grain boundaries (Fig. 2c), and (ii) a random distribution of microscopic voids both in the grain interior and along the grain boundary region (Fig. 2d). Scanning electron microscopy

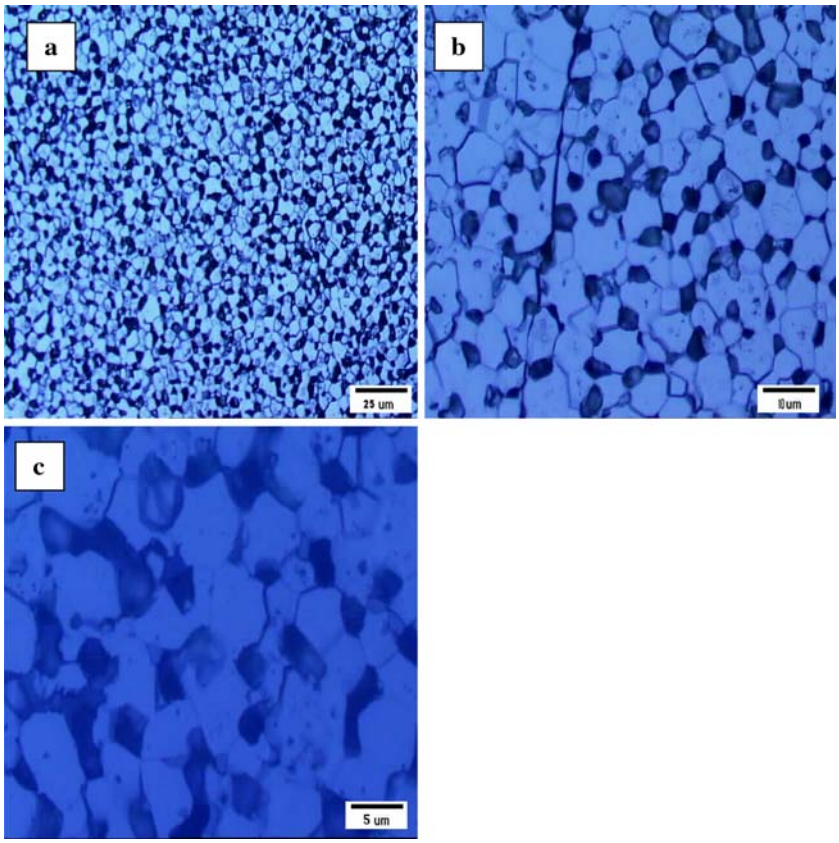

Fig. 8 Bright field optical micrographs of Sample #4, containing 1.0 wt.% carbon, showing: (a) Near uniform distribution of grains and random distribution of dark spots. (b) High magnification of (a) showing size and shape of the dark spots. (c) A dark spot is an agglomeration of fine microscopic void: i.e., a macroscopic void

observations confirmed the presence of a population of microscopic voids (Fig. 3a) and microscopic cracks (Fig. 3b) distributed through the microstructure of this ceramic sample. At the higher magnifications was also evident the occurrence of void coalescence along the grain boundary regions to form microscopic cracks (Fig. 3c), which are detrimental to mechanical properties, i.e., hardness.

4.2.2 Sample #2. The sample revealed a near uniform grain size distribution at low magnification (Fig. 4a). At the higher magnifications of the optical microscope revealed the grains irregular in shape (Fig. 4b) and a population of voids and cracks distributed randomly through the microstructure (Fig. 4 c). Further, the grains were found to be irregular in shape (Fig. 4d). Scanning electron microscopy observations revealed a network of fine microscopic voids distributed randomly through the microstructure of this sample (Fig. 5a). The network and close proximity of the microscopic voids in the ceramic matrix revealed a near-fibrous appearance (Fig. 5b). At regular intervals, the microscopic voids coalesce to form microscopic cracks that were distributed through the microstructure (Fig. 5c). The presence of sizeable volume fraction of processing-related defects suggests that the powder particles of this sample containing 0.1 wt.% carbon were not consolidated to its fullest density at the processing temperature (1850 °C) and pressure (50 MPa).

4.2.3 Sample #3. Low magnification electron microscope observation revealed a near uniform distribution of grains with a random distribution of dark spots indicative of agglomeration of the carbon particles, i.e., excess carbon content (Fig. 6a). At the higher magnifications in the optical microscope revealed the grains to be near spherical in morphology (Fig. 6b) with a random distribution of microscopic cracks and a population of voids of varying size (Fig. 6c). The microscopic cracking was dominant along the grain boundary regions. This is confirmed by scanning electron microscopy observations, which revealed cracking along the grain boundaries (Fig. 7a) containing a population of microscopic voids and the occurrence of void coalescence to form microscopic cracks at regions of the grain boundary triple junction (Fig. 7b).

4.2.4 Sample #4. Overall, examination of the microstructure at low magnifications revealed a near uniform grain size coupled with a random distribution of dark spots through the microstructure (Fig. 8a). At the higher magnifications, the irregular shaped dark spots (Fig. 8b) were identified to be an agglomeration of microscopic voids of varying size (Fig. 8c). The microstructure of this sample revealed evidence of less densification than the other two carbon-containing samples observed (Samples #2 and #3). Scanning electron microscopy observations revealed hexagonal shaped grains (Fig. 9a). At the higher magnifications was evident fine cracking along the grain boundary regions along with a population of microscopic voids (Fig. 9b).

For a single-phase ceramic material, the influence of sintering temperature on average grain size is expressed by the relationship (Ref 32).

$$G = G_o + K \cdot t^n,$$

where G is the average grain size, G_o is the initial grain size, t is the sintering time, and n is the growth co-efficient. Theoretically 'n' should be around 0.5. However, the occurrence and presence of processing related artifacts in the form of microstructural defects, such as: (a) fine microscopic pores, (b) a population of voids of varying size, and (c) microscopic cracks both on the surface and along the grain boundary regions, aids in retarding the growth of grains with a concomitant decrease in the growth coefficient 'n.' This relationship appears to be valid for the bulk samples of HfB_2 examined since a higher sintering temperature resulted in a lower density of the microscopic pores, the density of voids of varying size, and the presence of microscopic cracks caused as a direct result of the decrease in force required to move a grain boundary. The decrease in force is conducive for the growth of grains in the microstructure of this ceramic as was observed in both the optical microscope and scanning electron microscope.

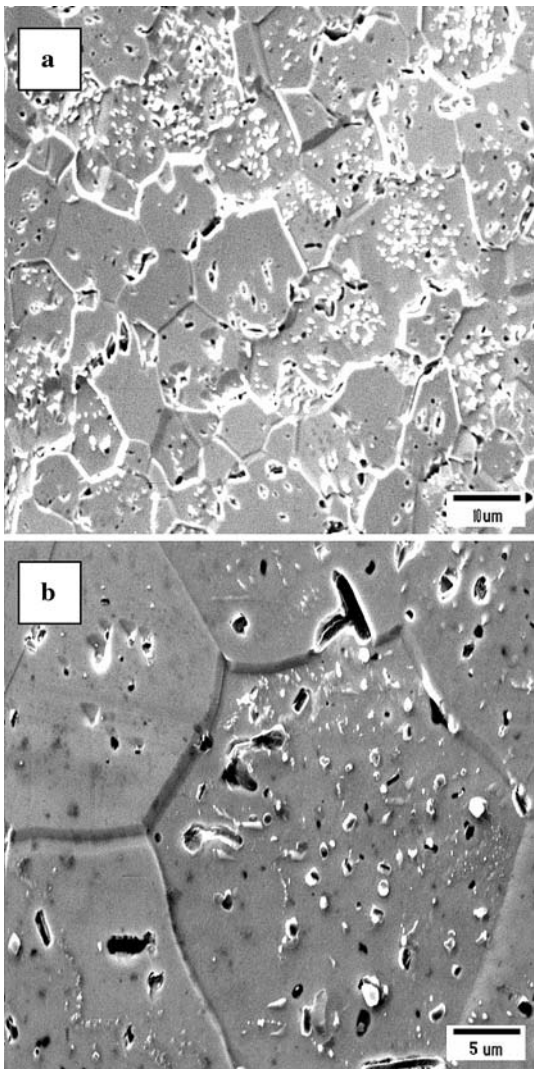

Fig. 9 Scanning electron micrographs of the surface of Sample #4 showing: (a) Near hexagonal shaped grains. (b) Cracking along the grain boundary regions and a population of microscopic voids

4.3 Microhardness

Knoop hardness measurements were made from edge-to-edge of the as-consolidated samples. The recorded microhardness value of a sample is a combination of the material's inherent resistance to indentation and the loss of strength (hardness) resulting from the presence of microscopic defects such as pores, voids and cracks. The Knoop hardness values are summarized in Table 4.

(i) Sample #1 containing no carbon content had a hardness of 413 H_k, whereas Sample #2 containing 0.1% carbon revealed a hardness of 300 H_K conforming well with the presence of a sizeable volume fraction of pores, voids, and micro cracks in the microstructure.
(ii) Sample #3 containing 0.5% carbon revealed a significantly higher hardness than the Sample #1, which contained no carbon.
(iii) Sample #4 containing 1% carbon had an average hardness of 448 H_K, which is much higher than the sample containing no carbon and 0.5% carbon.

All of the samples except Sample #2, which contained a sizeable number of processing related artifacts, such as: (i) pores, (ii) a population of voids, and (iii) microscopic cracks in the microstructure, revealed a hardness value commensurate with composition and processing history. The influence of

Table 4 Knoop microhardness for above indentation measurements (Indentation load = 500 g load; Dwell time: 10 s)

Sample number	Hardness trials					Average
	1	2	3	4	5	
1	384.65	414.55	396.2	448.2	421	412.92
2	329.25	312.1	271.1	274.5	312.1	299.81
3	455.35	478	421	421	421	439.27
4	441.1	478	414.5	455.35	455.35	448.86

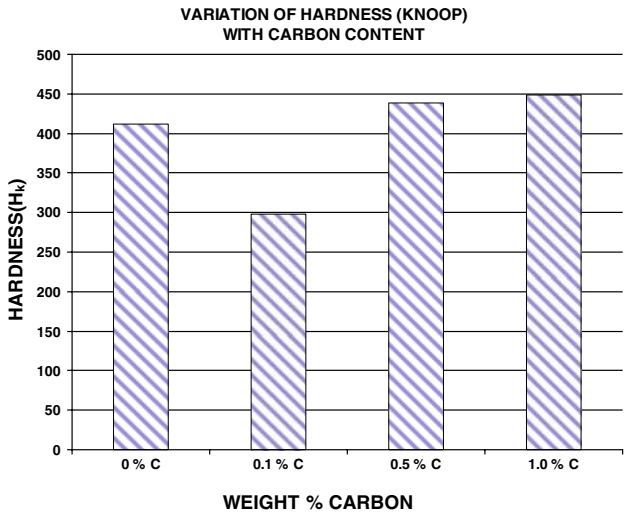

Fig. 10 Bar graph showing the influence of carbon content on Knoop microhardness of the hafnium boride samples

carbon content on microhardness is depicted in the bar graph in Fig. 10.

5. Conclusions

A comprehensive examination of the bulk samples of HfB_2 did provide an insight into establishing an understanding of the influence of consolidation temperature and carbon content on microstructural development of the bulk sample of the single phase ceramic. The results are summarized as follows:

1. The consolidation time (15 min) and temperature of 1850 °C was found to be suitable from the standpoint of compaction and density.
2. Sample #1 with no carbon additive revealed the lowest density commensurate with the presence of processing related artifacts in the microstructure. Sample #2 containing 0.1 wt.% C revealed a lower microhardness due to the presence of a large number of processing related artifacts but significantly higher density.
3. Sample #3 containing 0.5 wt.% carbon revealed a higher hardness and high compaction density even at the lower consolidation temperature (1750 °C). This is attributed to the absence of a large volume fraction of pores, voids, and cracks.
4. Since all the samples revealed evidence of microscopic pores and voids, the occurrence of gas evolution during consolidation cannot be ruled out. The gases arise from the presence of carbon and its reaction with the impurities, which is exacerbated by the locally high temperatures resulting in the formation and evolution of gaseous byproducts and their resultant entrapment during consolidation and cooling.

Acknowledgments

The authors extend most sincere thanks and appreciation to the unknown reviewers for their critical comments, corrections, and useful suggestions have helped strengthen the technical merit of this manuscript.

References

1. F. Monteverde and A. Bellosi, *Adv. Eng. Mater.*, 2004, **6**(5), p 331–335
2. L. Kaufman and H. Nesor, *Stability Characterization of Refractory Materials under High Velocity Atmospheric Flight Conditions*, AFML-TR-69–84, Part II, Vol. II: Facilities and Techniques Employed for Cold Gas/HotWall Tests, ManLabs, Inc., Cambridge, Mass., Sept. 1969
3. L. Kaufman and H. Nesor, *Stability Characterization of Refractory Materials under High Velocity Atmospheric Flight Conditions*, AFML-TR-69-84, Part II, Vol. III: Facilities and Techniques Employed for Cold Gas/Hot Wall Tests, MansLabs, Inc., Cambridge, Mass., Sept. 1969
4. L. Kaufman and H. Nesor, *Stability Characterization of Refractory Materials under High Velocity Atmospheric Flight Conditions*, AFML-TR-69- 84, Part III, Vol. I: Experimental Results of Low Velocity Cold Gas/Hot Wall Tests, ManLabs, Inc., Cambridge, Mass., Sept. 1969
5. R. Perkins, L. Kaufman, and H. Nesor, *Stability Characterization of Refractory Materials under High Velocity Atmospheric Flight Conditions*, AFML-TR-69-84, Part III, Vol. II: Experimental Results of High Velocity Cold Gas/HotWall Tests, Man-Labs, Inc., Cambridge, Mass., Sept. 1969
6. L. Kaufman and H. Nesor, *Stability Characterization of Refractory Materials under High Velocity Atmospheric Flight Conditions*, AFML-TR-69-84, Part III, Vol. III: Experimental Results of High Velocity Hot Gas/ColdWall Tests, ManLabs, Inc., Cambridge, Mass., Sept. 1969
7. I.E. Campbell and E.M. Sherwood, *High-Temperature Materials and Technology*, Wiley, New York, 1967
8. (a) J.B. Berkowitz-Mattuck, *J. Electrochem. Soc.,* 1966, **113**, p 908. (b) J.B. Berkowitz-Mattuck, *J. Electrochem. Soc.,* 1966, **114**, p 1030
9. W.C. Tripp and H.C. Graham, *J. Electrochem. Soc., Solid State Sci.*, 1971, **118**(7), p 1195
10. R.A. Cutler, *Engineering Properties of Borides in Engineering Materials Handbook, Ceramics and Glasses*, Vol. 4. ASM International, Metals Park, Ohio, 1987
11. E.L. Courtright, H.C. Graham, A.P. Katz, and R.J. Kerans, "Ultrahigh Temperature Assessment Study of Ceramic Matrix Composites," Report No. WL-TR-91-4061, Wright-Patterson AFB, Ohio, 1991
12. C.B. Bargeron, R.C. Benson, R.W. Newman, A.N. Jette, and T.E. Phillips, *Johns Hopkins APL Tech. Dig.*, 1993, **14**(1), p 293
13. K. Upadhya, J.M. Yang, and W. Hoffman, *Bull. Am. Ceram. Soc.*, 1997, **76**(12), p 1–56
14. M.M. Opeka, I.G. Talmy, E.J. Wuchina, J.A. Zaykoski, and S.J. Causey, *J. Euro. Ceram. Soc.*, 1999, **19**, p 2405–2414
15. J. Fuller and M.D. Sacks (Guest Eds.), Special section on Ultra-High Temperature Ceramics (UHTC), *J. Mater. Sci.*, 2004, **39**, p 5885–6066
16. D.S. Wu, M.L. Lee, T.Y. Ly, and R.H. Horng, *Mater. Chem. Phys.*, 1996, **45**, p 163–166
17. Y.D. Blum and H.J. Kleebe, Chemical reactivities of hafnium and its derived boride, carbide and nitride compounds at relatively mild temperature, *J. Mater. Sci.*, 2004, **39**, p 6023–6042
18. L. Kaufman, AFML Report No. RTD-TDR-63–4096, Part II, Feb. 1965
19. (a) E. Rudy and ST. Windisch, U.S. Air Force Tech. Doc. Report AFML-TR-65-2, Part 1, Vol. IX, Feb. 1966, p 1. (b) E. Rudy and J. Progulski, *Planseeber Pulvermet*., 1967, **15**, p 13
20. R. Kalyanaraman, S. Yoo, M.S. Krupasankara, T.S. Sudarshan, and R.J. Dowding. *Nanostruct. Mater*., 1998, **10**, p 1379
21. S.H. Yoo, T.S. Sudarshan, K. Sethuram, G. Subhash, and R.J. Dowding, *Powder Metal.*, 1999, **42**(2), p 181–182
22. R. Ka1yanaraman, S.H. Yoo, M.S. Krupashankara, T.S. Sudarshan, and R.J. Dowding, *Powder Metal.*, 2000, **43**(4), p 380–385
23. B.G. Ravi, O.A. Omotoye, T.S. Srivatsan, M. Petraroli, and T.S. Sudarshan, *J. Alloys Comp.*, 2000, **299**, p 292–296
24. T.S. Srivatsan, B.G. Ravi, A.S. Naruka, L. Riester, M. Petraroli, and T.S. Sudarshan, *J. Powder Technol.*, 2001, **114**, p 136–144
25. T.S. Srivatsan, B.G. Ravi, A.S. Naruka, L. Riester, S. Yoo, and T.S. Sudarshan, *Mater. Sci. Eng., Ser. A*, 2001, **A311**, p 22–27
26. T.S. Srivatsan, B.G. Ravi, A.S. Naruka, L. Riester, S. Yoo, and T.S. Sudarshan, *Mater. Sci. Eng., Ser. A*, 2001, **A311**, p 22–27
27. B.R. Klotz, K.C. Cho, and R.J. Dowding, *Mater. Manuf. Process*, 2004, **19**(4), p 641–650
28. K.Y. Cho, R.H. Woodman, B.R. Klotz, and R.J. Dowding, *Mater. Manuf. Process*, 2004, **19**(4), p 619–630
29. T.S. Srivatsan, G. Guruprasad, D. Black, M. Petraroli, R. Radhakrishnan, and T.S. Sudarshan, *Powder Technol.*, 2005, **159**, p 161–167
30. T.S. Srivatsan, G. Guruprasad, D. Black, M. Petraroli, R. Radhakrishnan, and T.S. Sudarshan, *J. Alloys Compounds*, 2006, **413**, p 63–72
31. H. Chandler, *Hardness Testing*, ASM International, 1999, p 72
32. W.D. Kingery, *Introduction to Ceramics*. Wiley, New York, 1976, p 411